Supplement of Atmos. Chem. Phys., 23, 5419–5433, 2023
https://doi.org/10.5194/acp-23-5419-2023-supplement

Atmospheric Chemistry and Physics
Open Access
EGU

Supplement of

Multiple pathways for the formation of secondary organic aerosol in the North China Plain in summer

Yifang Gu et al.

Correspondence to: Ru-Jin Huang (rujin.huang@ieecas.cn)

Table S1. Summary of Mass Concentrations of $PM_{2.5}$ Species and OA Components ($\mu g\ m^{-3}$), Mixing Ratios of gas-phase pollutants, and meteorological parameters in the Summer Studies in Handan.

	Handan Summer			
	All	P1	P2	P3
Total	37.3±19.0	29.3±12.7	36.0±14.7	64.1±29.4
OA	19.6±5.5	15.4±3.2	19.8±4.7	25.0±6.2
HOA	2.4±2.1	2.2±1.5	2.6±2.5	1.7±1.1
COA	3.7±2.6	4.6±3.3	3.1±2.2	3.4±2.8
primary-related SOA	1.0±1.2	1.0±1.3	1.0±1.2	0.7±1.4
fresh SOA	3.5±2.5	3.5±1.3	4.0±2.3	5.5±2.7
O_x-initiated SOA	6.1±3.3	6.1±1.9	7.3±3.1	5.4±2.4
aqSOA	3.9±3.5	2.9±2.2	1.8±2.0	8.3±6.3
Sulfate	7.2±4.9	5.9±5.8	7.1±4.0	11.8±6.2
Nitrate	4.3±6.3	3.5±2.9	3.0±4.4	14.9±11.3
Ammonium	2.7±2.5	2.2±1.9	2.4±1.7	6.5±4.1
Chloride	0.4±0.6	0.3±0.3	0.4±0.6	1.0±1.1
BC	3.1±2.0	2.0±1.2	3.3±1.9	4.9±2.4
CO(ppm)	0.8±0.7	0.6±0.6	0.8±0.8	1.3±0.5
NO_2(ppb)	14.4±9.9	11.8±5.3	15.6±11.7	15.9±5.4
SO_2(ppb)	4.0±4.6	2.4±2.5	5.2±5.5	2.2±1.5
O_3(ppb)	54.0±22.8	24.0±14.5	49.5±29.1	32.2±24.6
WS(m/s)	1.5±1.0	1.7±1.1	1.6±1.0	1.0±0.6
WD(°)	187.1±121.8	223.1±126.6	168.2±111.5	201.9±124.4
T(℃)	25.0±4.3	22.3±2.8	26.4±4.0	23.1±2.6
RH(%)	66.3±19.4	79.4±13.0	57.7±17.5	83.7±12.5
ALWC	21.4±51.3	22.6±48.0	8.4±15.8	95.4±114.2

Table S2. Concentrations of the main chemical components in PM_1/$PM_{2.5}$ during summer and winter observations in recent years.

Sites	OA	SO4	NO3	NH4	Cl	BC	PM	PM_1	NR-PM_1	$PM_{2.5}$
Our study	19.0	7.2	4.3	2.7	0.4	3.1				36.7
2013 Summer, Handan (Zhao et al., 2019)		16.1	16.5	7.3	3.3					95.6
2017 Summer, Handan (Zhao et al., 2019)		13.4	5.0	6.2	0.7					64.8
2015 winter, Handan (Li et al., 2017)	81.2	28.1	26.1	21.4	16.6	9.4		187.6	173.4	
2018 Summer, Beijing (Xu et al., 2019b)	12.7	6.5	7.4	4.3	0.2				31.1	
2018 Summer, Beijing (Chen et al., 2020)	12.2	3.9	2.5	2.2	0.1	3.2		24.1		
2019 Summer, Beijing (Chen et al., 2020)	9.3	4.5	2.8	2.5	0.2			19.3		
2019 Summer, Xian (Duan et al., 2020)	14.0	3.9	2.8	1.7	0.1					22.5

Table S3. Elemental ratios and OM:OC ratios in OA obtained from field observations at urban and rural/suburban sites. The ratios are corrected by the "improved-ambient" method (Canagaratna et al., 2015).

sites	site types	seasons	H:C	O:C	OM:OC	ref
our study	urban	summer 2019	1.58	0.75	2.17	
	suburban	summer 2018	1.67	0.54	1.89	Chen et al.2020b
Beijing	urban	summer 2012	1.63	0.53	1.88	Hu et al.2017
		winter 2013	1.52	0.47	1.79	
		summer 2011	1.61	0.56	1.91	Hu et al.2016a
		winter 2010	1.65	0.32	1.58	
Xi'An	urban	summer 2019	1.64	0.58	1.96	Duan et al. 2020
Hangzhou	urban	Before G20	1.78	0.39	1.69	Li et al., 2017
		During G20	1.65	0.58	2.03	
		After G20	1.69	0.51	1.84	
Lanzhou	urban	winter 2014	1.55	0.28	1.51	Xu et al., 2016
		summer 2012	1.49	0.33	1.58	
Guangzhou	suburban	winter 2014 Nov.	1.63	0.53	1.87	Qin et al., 2017
		winter 2014 Dec.	1.65	0.53	1.87	
Kaiping	suburban	autumn 2008	1.64	0.6	1.94	Huang et al.,2011
Heshan	suburban	autumn 2010	1.65	0.51	1.83	Gong et al., 2012
Shenzhen	urban	winter 2009	1.83	0.39	1.71	He et al.,2011
		summer 2011	1.74	0.45	1.81	Gong et al., 2012
Shanghai	urban	summer 2010	1.92	0.4	1.69	Huang et al.,2012
Ziyang	suburban	winter 2013	1.56	0.65	2.02	Hu et al.2016b
Jiaxing	suburban	summer 2010	1.94	0.36	1.67	Huang et al.,2013
		winter 2010	1.73	0.43	1.75	
HKUST	suburban	summer 2011	1.48	0.64	1.93	Li et al., 2015
		winter 2012	1.53	0.53	1.8	
MongKoK	urban	summer 2013	1.83	0.26	1.5	lee et al., 2015
Fresno.CA (US)	urban	winter 2010	1.75	0.35	1.63	Ge et al. (2012)
Riverside,CA (US)	urban	summer 2005	1.71	0.44	1.73	Docherty et al. (2011)
Korea	urban	winter 2019	1.79	0.37	1.67	Kim et al. 2017
Oregon (US)	No BB	summer 2013	1.48	0.84	2.26	Zhou et al., 2017
	BB infl		1.49	0.77	2.16	
	BB plm		1.53	0.69	2.06	

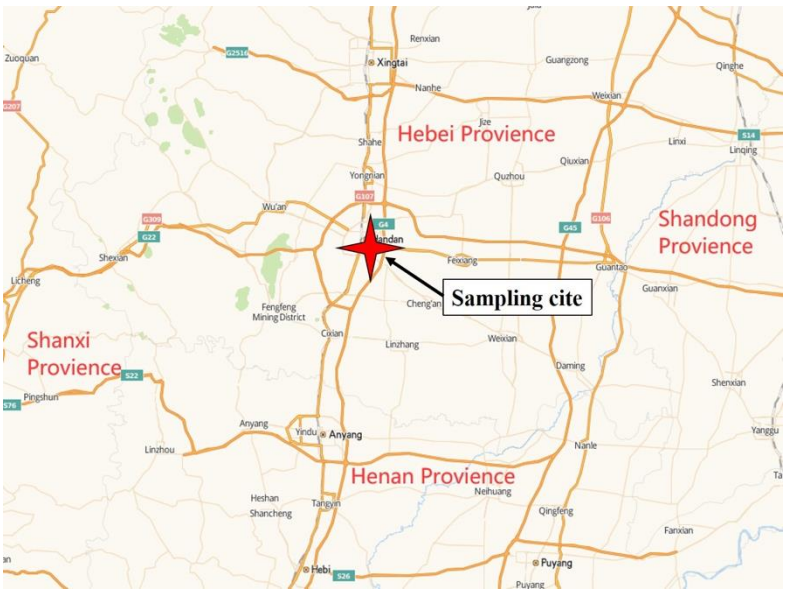

Fig. S1 Location of the $PM_{2.5}$ sampling site in Handan (the red star). The base map image was derived from AutoNavi Maps (Image © 2022 AutoNavi-GS).

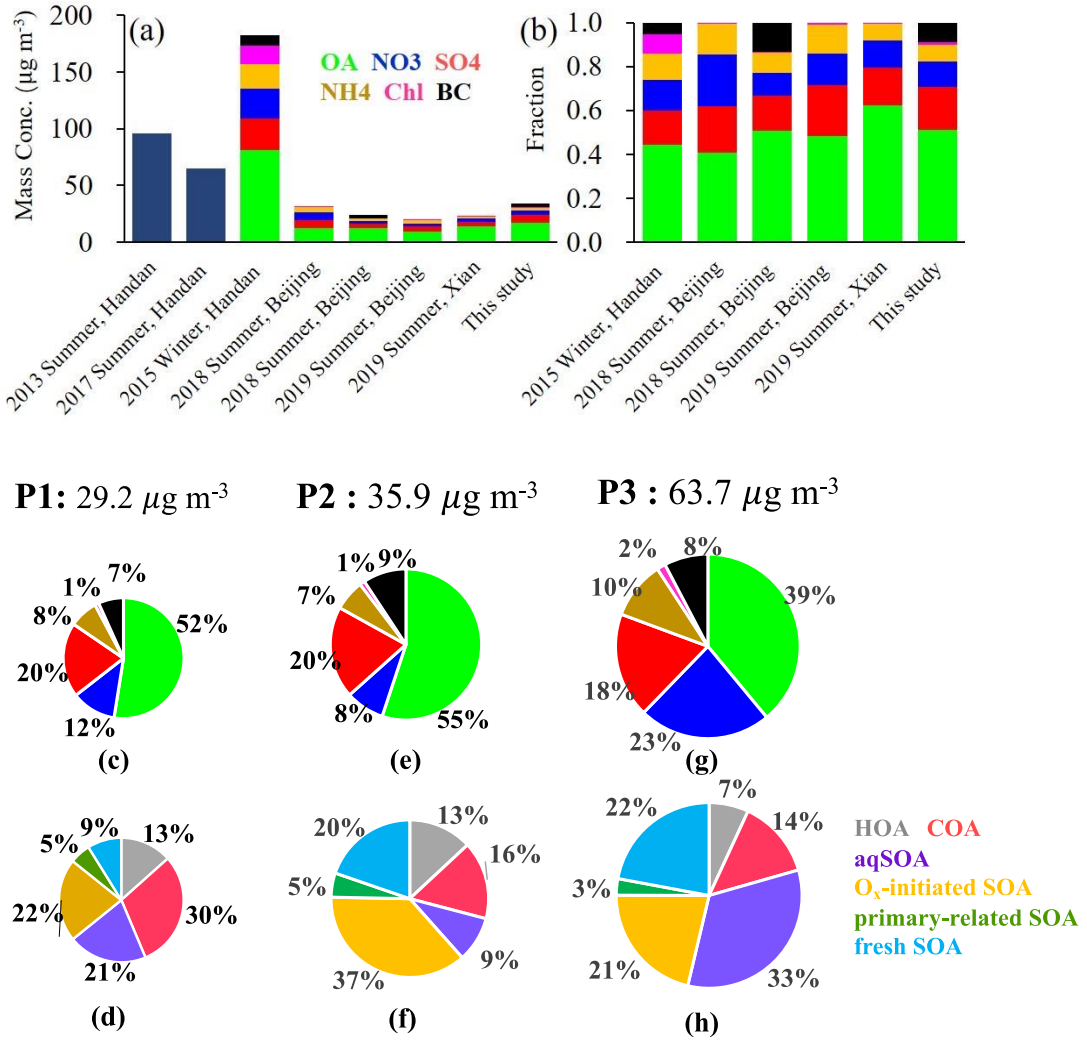

Fig. S2 Concentrations (a) and fractions (b) of main chemical components in PM_1/$PM_{2.5}$ during summer and winter observations in the NCP in recent years. The data and references are available in Table S2 of the Supplement. Fractions of main chemical components of $PM_{2.5}$ and OA in reference events (P1: c & d), high O_x period (P2: e & f) and high RH period (P3: g & h).

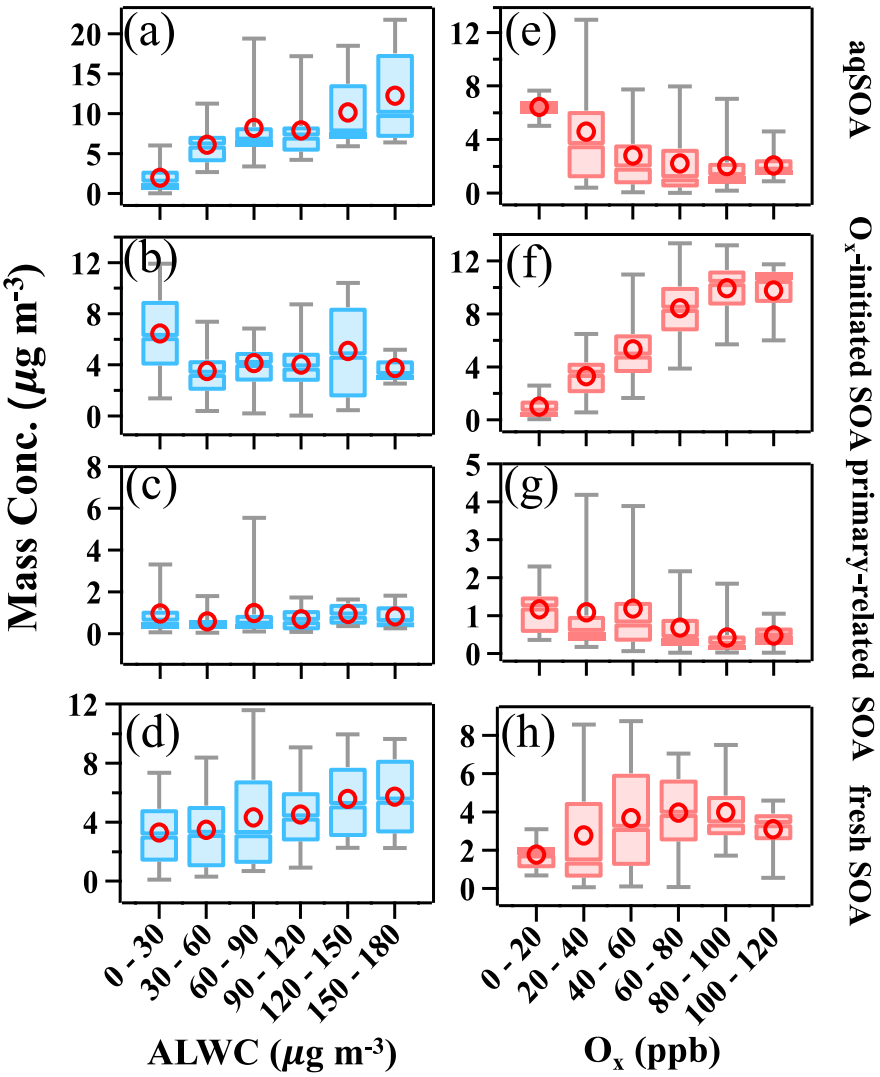

Fig. S3 Variations of the mass concentrations of aqSOA, O_x-initiated SOA, primary-related SOA and fresh SOA as functions of ALWC (a~d) and O_x (e~h). The data were binned according to the ALWC (30 μg m^{-3} increment) or O_x concentration (10 ppb increment), and mean (circle), median (horizontal line), 25th and 75th percentiles (lower and upper box), and 10th and 90th percentiles (lower and upper whiskers) are showed for each bin.

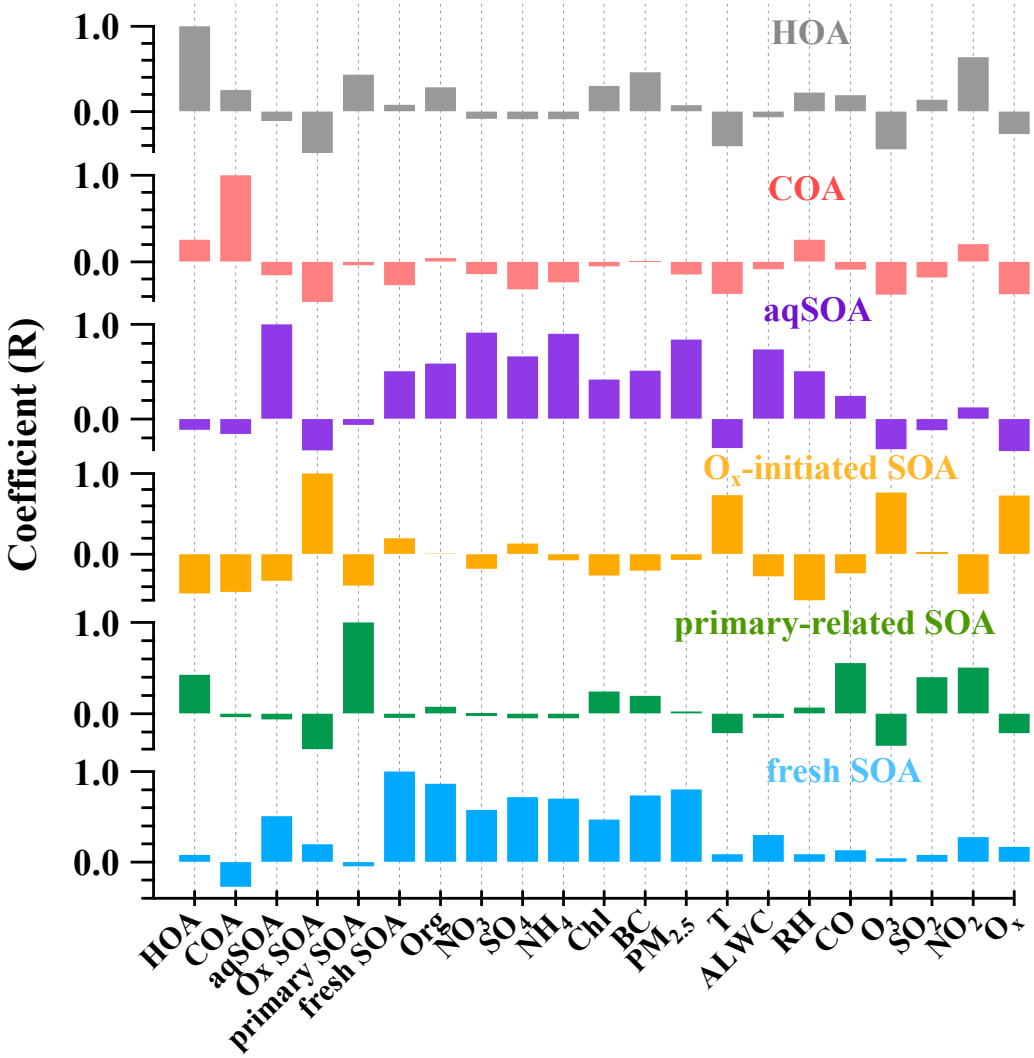

Fig. S4 Correlation between the resolved OA factors and other chemical components in $PM_{2.5}$, gas-phase pollutants, and meteorological parameters.

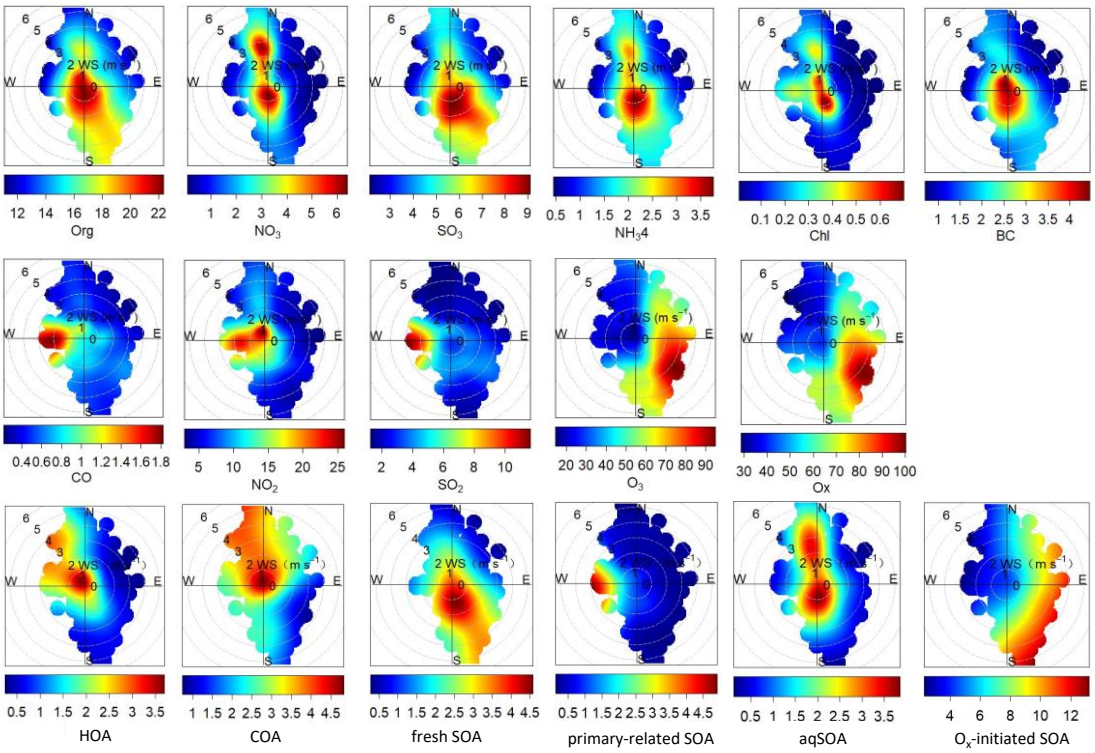

Fig. S5 Polar plots that illustrate the variations of the hourly averaged concentrations of gases pollutants, $PM_{2.5}$ species and OA sources as a function of wind speed (m s^{-1}) and wind direction (°).

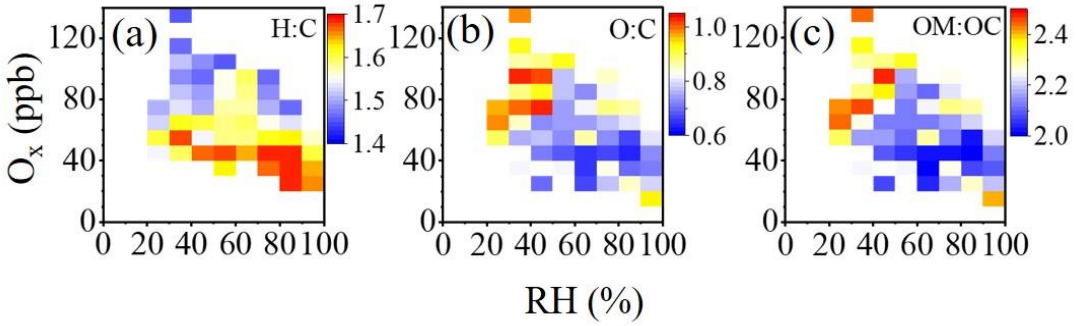

Fig. S6 RH- and O_x-dependent distributions of (a) H:C, (b) O:C and (c) OM:OC ratios. Grids with the number of points less than five were excluded.

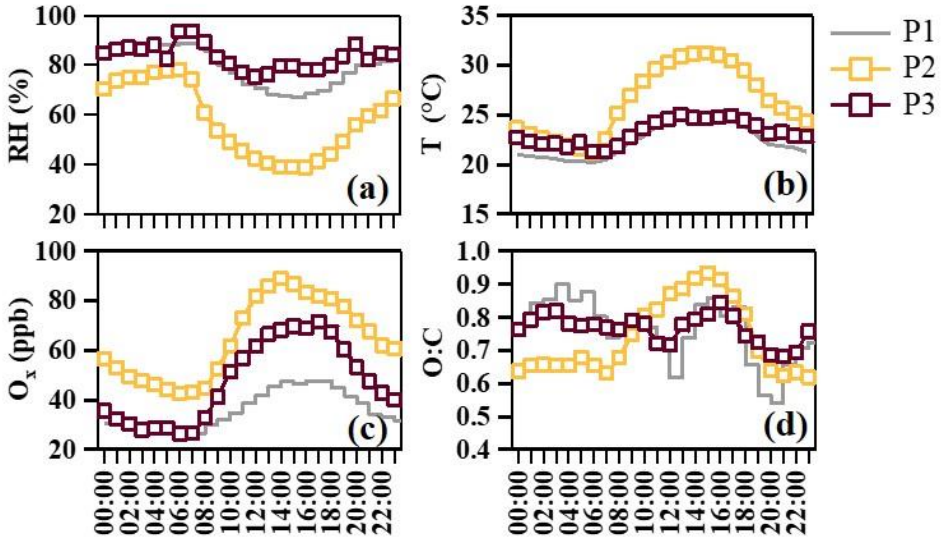

Fig. S7 Diurnal patterns of (a) RH, (b) temperature, (c) O_x and (d) O:C ratios in reference events (P1), high O_x period (P2) and high RH period (P3).

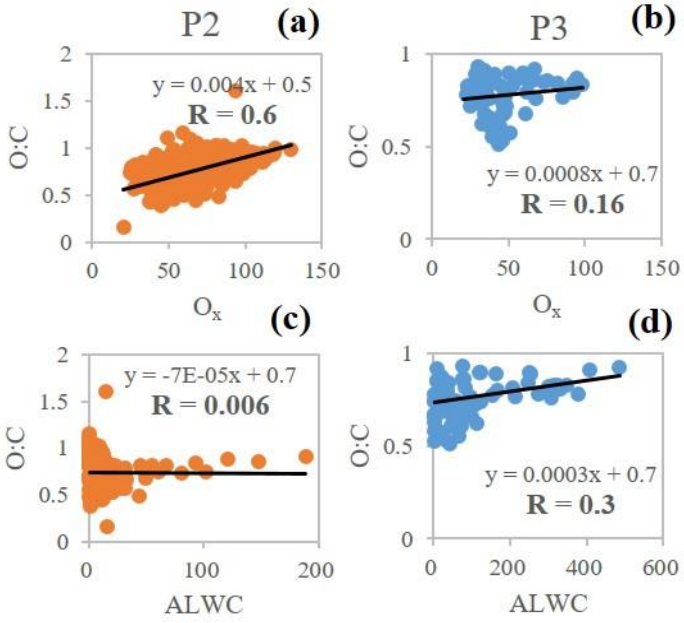

Fig. S8 Relationship between O:C ratios and O_x/ALWC in high O_x period (P2: a & c) and high RH period (P3: b & d) during this campaign.

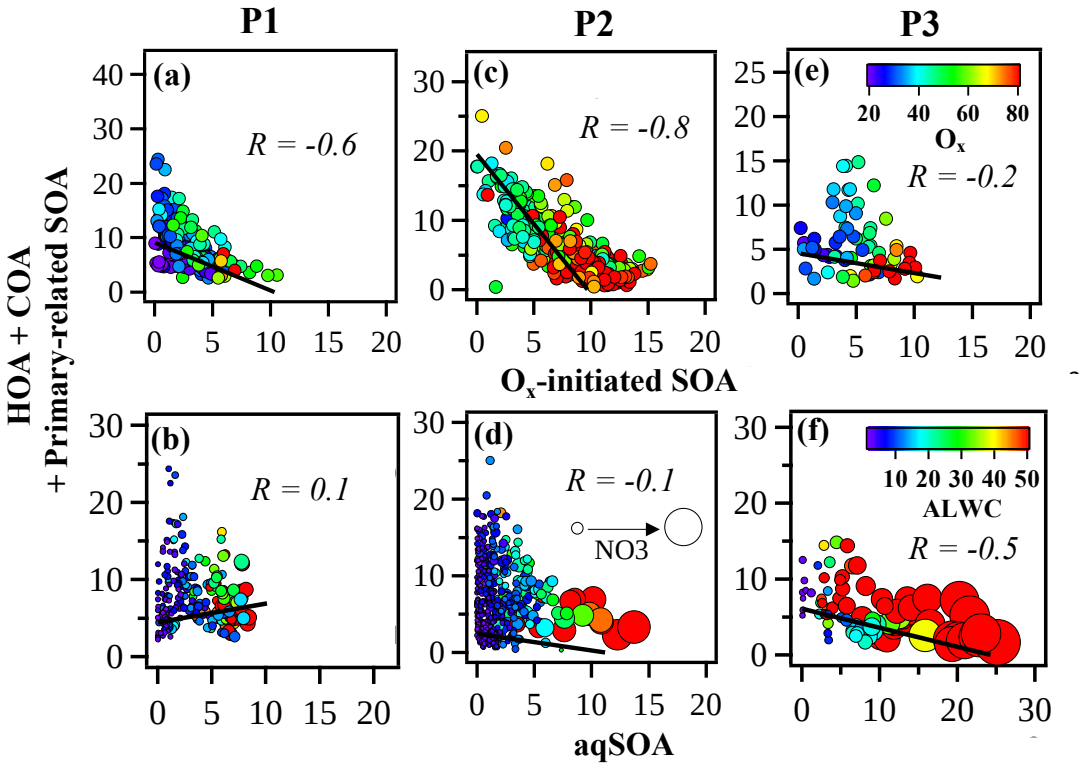

Fig. S9 (a) Relationship between aqSOA and the sum of POA and primary-related SOA colored by ALWC (μg m^{-3}) and sized by NO3 (μg m^{-3}); (b) Relationship between O_x-initiated SOA and the sum of POA and primary-related SOA colored by O_x (ppb) in reference period (P1: a&b), high O_x period (P2: c&d) and high RH period (P3: e&f) during this campaign.

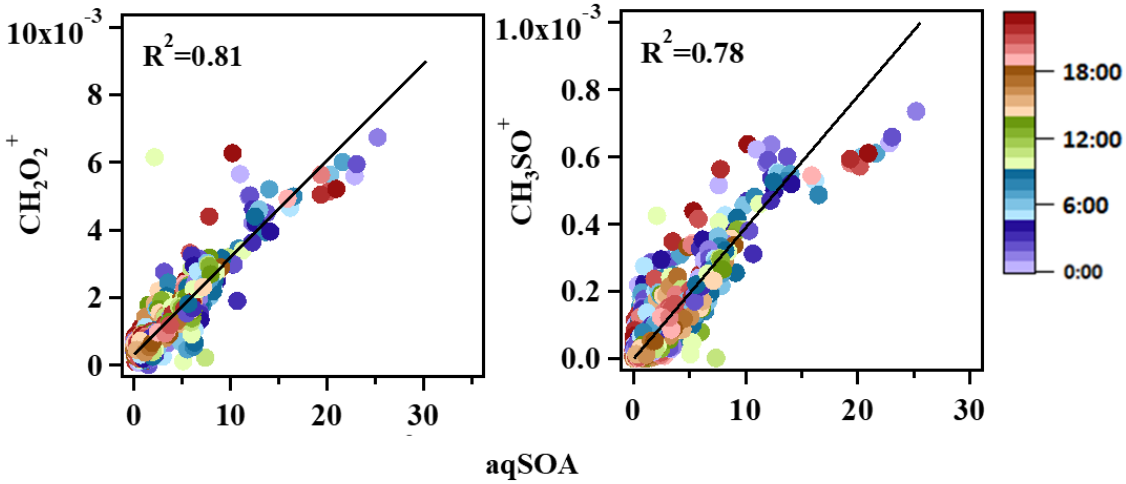

Fig. S10 Correlation between aqSOA (μg m^{-3}) with $CH_2O_2^+$ at *m/z* 46 and CH_3SO^+ at *m/z* 63 (μg m^{-3}).

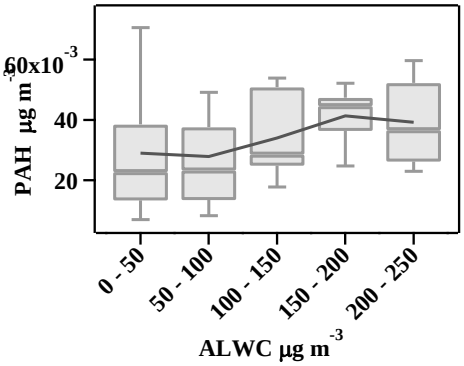

Fig. S11 Mass concentration of PAHs ions as a function of ALWC.

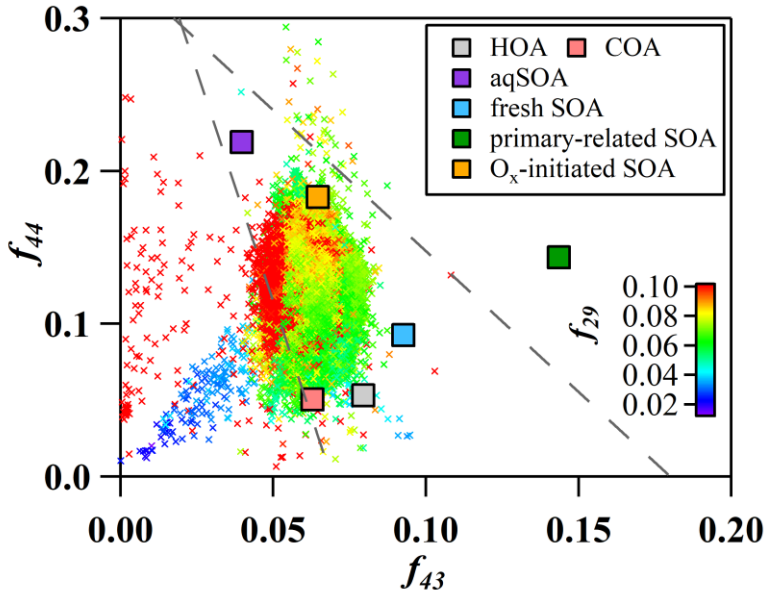

Fig. S12 Triangle plots of f_{44} versus f_{43}, the dash lines were adopted from Ng et al. (2010). All the data and related references can be found in Table S3.

Supplementary information

1.1

In the studied time period, POA (6.1 ±3.61 μg m^{-3}) contributed 30.6% to the bulk OA, including the hydrocarbon-like OA (HOA, 12.2%) and cooking OA (COA, 19.1%) in summer of Handan. The results are consistent with the results in summer 2017 and 2018 from Beijing (Xu et al 2019b).

HOA

The spectrum of HOA is substantially contributed by alkyl fragments ($C_nH_{2n+1}^+$ and $C_nH_{2n-1}^+$, Fig. 1), major ions include $C_3H_7^+$, $C_4H_9^+$, and $C_5H_{11}^+$ (Zhao et al., 2019; Xu et al., 2019a; Sun et al., 2016; Elser et al., 2016; Zhang et al., 2014; Ng et al., 2011), which is consistent with the previous studies (Canagaratna et al., 2004; Ng et al., 2010). HOA had a relative low O:C ratio of 0.14 and high H:C ratio of 1.77. On average, it accounted for 12.2% of total OA (Fig. S2a) in Handan, with the absolute concentration of 2.4 ±2.1 μg m^{-3}, which was two times lower than that in Beijing (35%) at the same time period of 2018 (Chen et al., 2020a). The low HOA fraction was consistent with previous study, which revealed that transportation was a minor source of atmospheric particles in Handan compared to Beijing (Wang et al., 2014).

High correlations were also observed between the time series of HOA with BC (R=0.5) and NO_2 (R=0.6, Fig. S4), supporting the vehicle emission related origins of HOA reported in the previous studies (Lanz et al., 2007; Docherty et al., 2011). The polar plots (Fig. S5) demonstrated higher concentrations of HOA under relatively low WS (< 2.0 m s^{-1}), which was very similar with BC, supporting the fact that HOA is a freshly locally-emitted vehicle OA. HOA exhibited slightly enhanced peaks in the morning (6:00-7:00 local time, LT) and prominent peaks during nighttime (19:00-22:00 LT) when the traffic jam happened (Fig. 6). However, these kinds of variations were less pronounced in P1 and P3 (Fig. 6), which might because the high WS and RH had influence to such local sources. Hence the stagnant meteorological conditions would result in accumulation of local sources during this measurement period. It should be noted that the fraction of HOA is lower during P3 (7%) compared with P1 and P2, this may be attributed to the large fraction of SOA (Fig. S2). The average HOA/BC ratio was 0.8, close to other cities in China e.g., Xianghe (0.91) (Sun et al., 2016), which was between those for diesel trucks (0.5) (Ban-Weiss et al., 2008) and light-duty vehicles (1.4).

COA

The COA mass spectrum was characterized by higher ratio than HOA between f_{55} ($C_4H_7^+$+$C_3H_3O^+$) and f_{57} ($C_4H_9^+$+$C_3H_5O^+$) (Mohr et al., 2012), and the spectral pattern was

relatively constant among different years. The O:C and H:C ratios of COA were 0.18 and 1.57, respectively, suggesting their primary feature (Xu et al., 2016). On average, the mass contribution of COA to OA was 19.1% (Fig. S2a), which was close to that in the summer of 2018 (15%) in Beijing (Xu et al., 2019b).

The most pronounced feature of COA (Fig. 6) is its clearly enhanced diurnal peaks around morning (6:00–7:00 LT), noon (12:00–13:00 LT) and late evening (19:00–20:00 LT), corresponding to the common meal hours which was consistent with previous studies of other regions of NCP (Sun et al., 2016; Sun et al., 2018;. During these meal hours, COA account for over 20% ~ 30% of total OA (Fig. S2d), signifying the importance of cooking sources in aerosol mass concentrations in urban areas of China.

Note that during the different periods, this mass fractions of COA to total OA present stable trend (14~16%) during P2 and P3, indicating that cooking styles remained consistent and local accumulation was not the major haze source during the measurement period (Fig. S2). While during the clean periods of P1 with wind, it increased to 30%, which was the largest contributor to OA. Moreover, the diurnal pattern of COA show very similar variations from three periods (Fig. 6) with the highest mass concentration during P1. This significant increase of COA is probably associated with the wind from southwestern where more residential areas with enhanced domestic cooking activities.

1.2

Characteristics of SOA sources

SOA accounted for 68.7% to total OA, four SOA factors were resolved depending on the oxidation state, which correspond to aged SOA and fresh SOA respectively (Jimenez et al., 2009). One factor is attributed to aqueous-phase chemistry (aqSOA) and the other to photo-oxidation chemistry (O_x-initiated SOA), while fresher factor is produced by fresh-source (fresh SOA), and the other considered as oxidized primary sources denoted as primary-related SOA. Although all of the SOA factors were characterized by higher *m/z* 44 (CO_2^+) and *m/z* 28 (CO^+) signal, their mass spectrum and temporal trends were noticeably distinguishable, corresponding to different formation mechanism, which will be discussed in the following section.

aqSOA

The aqSOA was identified as it increased with ALWC but decreased with O_x (Fig. S3), which might be produced in the aqueous-phase events and influenced by aqueous-phase chemistry. The aqSOA exhibits the highest O:C ratios of all factors (0.7) and a higher f_{CO2+} to the total signal of 21.7%, but a low H:C ratio of 1.24 (Fig. 1). On average, the mass concentration of aqSOA consisted 15.2% of the total OA and 22.1% of the SOA (Fig. S2a, b). Good correlations

were found between aqSOA and nitrate (R= 0.9), as well as ammonium (R= 0.9, Fig. S4) (Zhang et al., 2007; Aiken et al., 2009 and Huang et al., 2010). The high correlation with nitrate may be attributed to their similar precursors and formation pathways. It is also clear that their polar plot patterns are similar (Fig. S5) with two originations of nitrate and aqSOA were observed in our study. Results showed that the local origination associated with low wind speed (< 1.0 m s^{-1}) had a high concentration up to 4 μg m^{-3}, and the regional origination was associated with relatively high wind speed (> 2.5 m s^{-1}) derived from the northern regions (Fig. S5), suggesting that there were mixing regional and local sources for nitrate and aqSOA. This supports the aqSOA is relatively aged in ambient air and influenced by the combination of local formation and regional transport (Lanz et al., 2007; Hayes et al., 2013;Chen et al., 2021).

The aqSOA contributed a major fraction of 33.3 % to the total OA during P3 (peak concentration: 25.2 μg m^{-3}; peak fraction: 65.3%), pointing the faster SOA production through aqueous-phase chemistry during this specific haze event compared to P1 (20.5%) and P2 (9.4%). In addition, the ALWC and aqSOA were strongly correlated (R=0.7, Fig. S4), and both were shown dramatically enhancement during P3 event. This indicates that aqSOA was either formed via aqueous phase reactions or absorbed/dissolved into aerosol liquid water. Previous studies also showed that high RH in summer facilitated the transformation of HNO_3 into aqueous-phase and increased nitrate concentrations substantially (Sun et al., 2013; Sun et al., 2015). Due to the high NO_2 concentration and high RH in this period, particulate nitrate was produced during this regional transport homogeneously and heterogeneously, resulting in water uptake and high LWC in the aerosol phase. The high ALWC in turn facilitated further heterogeneous formation of nitrate. This positive feedback provided favorable conditions for efficient aqueous chemistry and thus production of aqSOA (Kuang et al., 2020). Note that the strong correlation between aqSOA and ALWC was not driven solely by P3 event, rather, the two time series were remarkably well correlated throughout the entire campaign. This further supported the interpretation of aqSOA as characteristic of aqueous SOA production throughout the campaign, rather than being characteristic of only a single event.

O_x-initiated SOA

The O_x-initiated SOA presented an opposite trend with significant increase as O_x but decrease as ALWC (Fig. S3). O_x has been shown to be a conserved tracer to represent photo-oxidation chemistry (Xu et al., 2017). The relationship between O_x and photochemical SOA can offer insight into the formation mechanism of SOA associated with ozone production chemistry (Herndon et al., 2008). Therefore, when the mass concentration of O_x-initiated SOA showed a substantial increase as a function of O_x, it could be likely due to the enhanced secondary transformation went from less oxidized to more aged with the progression of atmospheric

photochemical aging, which were supported by the large O_3 fractions in O_x in summertime (Zhang et al., 2019). Such conclusions were further supported by tightly tracked time series of O_x-initiated SOA with O_3 (R = 0.8) and O_x (R = 0.7) (Fig. S4). Considering O_3 has become the primary air pollutant in summertime in the NCP and had caused the enhancement of atmospheric oxidation capacity (Chen et al., 2020b), the photochemical processing driven by O_3 might play an important role in the formation of O_x-initiated SOA.

The O_x-initiated SOA had the highest average mass concentration of 6.1 $\pm$ 3.3 μg m^{-3} among the OA factors, with the highest contribution to total OA (31%) and the SOA (45%) during observation time, suggesting the predominate role of this factor (Fig. S2). The O_x-initiated SOA was oxidized with an O:C ratio of 0.67 and H:C ratio of 1.18, and it also had high CO_2^+ contribution of 17.9 %, which further suggested that the atmospheric oxidation capacity during summer was strong. Similar to aqSOA, O_x-initiated SOA also showed large variations during different periods. It accounted the most of 36.9% to OA during P2, compared to other two periods (21.5% in P1 and 21.3% in P3, respectively), indicating that the enhancement of O_x-initiated SOA can leads to the development of SOA formation. The O_x-initiated SOA also had the similar spatial pattern with O_3 and O_x form the polar plots (Fig. S5), where high concentration associated with southeast wind originated from Shandong with relatively high wind speed of over 4 m s^{-1}, suggesting the typical feature of regional transport pollutants.

primary-related SOA

In terms of two fresh SOA factors, they were defined as less oxidized OOA by relative lower O:C, stronger intensity of *m/z* 43 (mainly $C_2H_3O^+$) and *m/z* 44 (mainly CO_2^+).

The primary-related SOA constituted the lowest contribution of 5% among all factors of the total OA and 7% of the SOA, however, it is still of particular interest in this study. It is characterized by both lower H:C (1.09) and O:C (0.54) ratios with CO_2^+ comprising 14.3%, which are higher than other POA factors, indicating a typical nature of less oxidized SOA. However, at *m/z* > 120, clear polycyclic aromatic hydrocarbons (PAHs) fragments are evident in mass spectrum of primary-related SOA (Fig. 1), as indicated by the presence of similar patterns of PAH-like ions in their mass spectra at *m/z* 152, 165, 178, 189, 202, 216, 226 + 228, 240 + 242, 250 + 252, 264 + 266, 276 + 278 and 288 + 290 (Dzepina et al., 2007). Previous AMS studies have observed pronounced peaks of PAHs ions in POA spectrum, such as CCOA (coal combustion) and BBOA (biomass burning) (Hu et al., 2016a;Zhao et al., 2019), but rarely in SOA. This observation implies that primary-related SOA may be link to the POA origin from domestic coal combustion (Xu et al., 2006). Through laboratory combustion studies using online aerosol mass spectrometry, they examined substantial ion signal at *m/z* > 100, which potentially link to the fragments of high molecular weight (HMW) species, was pronounced in

both oxidized POA (OPOA) and POA, indicating that POA can be oxidized by multiphase reactions forming OPOA and the degradation of HMW species from the oxidation process (Budisulistiorini et al., 2021). In our study, the similar signatures of PAH-like ions was also found in aqSOA at m/z > 150, but less pronounced in aqSOA compared to primary-related SOA, consistent with previous study in Beijing (Wang et al., 2021). The observation of PAH-likes ions in both primary-related SOA and aqSOA further indicated they might both originated from coal combustion or transformation by oxidized POA, and the oxidation of PAHs being involved in the conversion of primary-related SOA to aqSOA.

As it is shown in Fig. S4, primary-related SOA exhibited relative better correlations with some gaseous pollutants, such as CO (R = 0.6), NO_2 (R = 0.5), and was also consistent with the temporal pattern of HOA (R = 0.4), suggesting primary-related SOA might be transformed from locally primary emissions. In addition, primary-related SOA, had no significant increase trend with both ALWC and O_x (Fig. S3), but its pollution pattern was similar as some primary precursors such as CO, SO_2 and NO_2, where higher concentrations appeared with weak west wind (Fig. S5). Therefore, the major pathway of this primary-related SOA formation might be related to primary emission or the its transformation, which also supported by similar results obtained by Rivellini et al., (2020), who found the oxygenated part of combustion particles which was co-emitted with HOA and/or produced by oxidation of HOA rapidly could be oxygenated-HOA (O-HOA) or oxygenated-CCOA. Moreover, some SOA factors were defined as "urban-lifestyle SOAs" because it could derived from some POA exhaust such as vehicle and cooking through laboratory experiments (Zhang et al., 2021).

fresh SOA

The fresh SOA showed increase substantially as ALWC increasing, similar to aqSOA. Whereas it also showed slight increase trend following O_x when O_x < 100 ppb (Fig. S3). Therefore, both aqueous-phase chemistry and photochemical processing were thought to have positive impacts synchronously on formation of fresh SOA. In this study, CO_2^+ comprised at least in fresh SOA of 8.3%, corresponding with the lowest atomic O:C ratio of 0.41 and a highest atomic H:C ratio of 1.41 among the four SOA factors. These characteristics consistent with the global average of LO-OOA of 0.35 ± 0.14, Ng et al., 2010), demonstrating the it is more fresh SOA. Besides, Fig. S2 showed that fresh SOA consisted 18% of the total OA and 26% of the SOA. Note that the concentration of fresh SOA increased in every event following with OA increased no matter the aqueous-phase event and photochemical event under the stagnant conditions. Meanwhile, it was well correlated with total OA (R = 0.9), $PM_{2.5}$ (R = 0.8) and BC (R = 0.7, Fig. S4), as well as sulfate (R = 0.7). The sustained contribution from fresh SOA and covariations between fresh SOA with these species suggest that it was probably a mixed source which not just

dominantly driven by only one formation mechanism. Nevertheless, different pathways among P1, P2 and P3 lead to the progressive fractions of fresh SOA to total OA. Compared with P1, photochemical processing (P2) and aqueous-phase reactions (P3) strengthen to produce fresh SOA individually, but the influence driven by aqueous-phase reactions is much greater than photochemical processing.

1.3 Evolution of OA

The mass spectra of these four factors for $PM_{2.5}$ are dominated by *m/z* 44 (mainly $CO2^+$) (Fig. 1). However, their concentrations show very different temporal variations. The concentration of aqSOA correlates with NO3 (R= 0.9) and ALWC (R= 0.7), showing a steady increase as a function of ALWC (Fig. S4 and Fig. S3) which might indicate aqueous-phase chemistry. The aqSOA exhibits the highest O:C ratio of all factors (0.7) and more aged oxidation state, while the O:C ratio of O_x-initiated SOA remains high (0.67) but slightly lower compared to aqSOA. The O_x-initiated SOA presents an opposite trend with significant increase as function of O_x but decrease as function of ALWC (Fig. S3), suggesting the photochemical formation and further supported by tightly tracked time series of O_x-initiated SOA with O_3 (R = 0.8) and O_x (R = 0.7) (Fig. S4). The mass spectrum of the fresh SOA shows a high peak at m/z 43 (mainly $C_2H_3O^+$) (Fig. 1), corresponding to the lowest atomic O:C ratio of 0.41 and a highest atomic H:C ratio of 1.41 among SOA factors, which indicate its feature of fresher SOA. Note that the concentration of fresh SOA increased in every period with OA increase, and was well correlated with total OA (R = 0.9), $PM_{2,5}$ (R = 0.8) and BC (R = 0.7), as well as SO4 (R = 0.7) (Fig. S4), indicating that they were freshly emitted and less oxidized. The primary-related SOA in this study was of particular interest. It has relatively low O:C (0.54) and H:C (1.09) ratios, indicating a typical nature of less oxidized SOA. However, as shown in Fig. S4, primary-related SOA exhibits relative better correlations with some gaseous pollutants, such as CO (R = 0.6), NO_2 (R = 0.5), and was also consistent with the temporal pattern of HOA (R = 0.4), suggesting primary-related SOA might be transformed from locally primary emissions.

1.4 VK Diagram

During this campaign, the H:C and O:C ratios in this study showed little variation, with average values of 0.75 ± 0.09 and 1.58 ± 0.28, respectively (Fig. 8a). The H:C ratio in Handan was slightly higher than that in Hong Kong (1.48) and Lanzhou (1.49) but lower than those at urban sites in Shenzhen (1.83), MongKok (1.83), Shanghai (1.92) and Jiaxing (1.94) (He et al., 2011; Huang et al., 2012, 2013; Li et al., 2015; Lee et al., 2015; Xu et al., 2016). Also, a general consistency was observed for the O:C ratio which was higher than mostly other sites, except the site in Oregon (US) influenced by wildfire. Overall, this relatively low H:C ratio, high O:C ratios suggested that OA in summer of Handan had higher degree of oxygenation than those at

urban sites due to the progress of atmospheric photochemical aging, and also indicated the secondary portion having a substantial contribution to the bulk OA. Figure S6 shows a synergistically impact of RH and O_x to elemental ratios. For example, H:C increased with the decrease of O_x concentration and with the increase of RH, which indicated that photochemical process had a positive effect but aqueous-phase process had an opposite effect on the H:C of atmospheric O. As for O:C, higher O:C ratio was mainly observed with high concentration of O_x, highlighting the importance of photochemical process in aerosol oxidation during summer. Meanwhile, slightly higher O:C also occurred at high RH levels even though the low concentration of O_x. Previous studies have demonstrated that aqueous-phase reactions of low-volatility high-molecular weight species detected in the atmosphere, such as glyoxal (Waxman et al., 2013), methyglyoxal (Lim et al., 2013), glycolaldehyde (Schöne and Herrmann, 2014), pyruvic acid (Altieri et al., 2006), and methacrolein (Liu et al., 2012), were the important formation pathway of OA (Kroll and Seinfeld, 2008; Hallquist et al., 2009; Sun et al., 2010; Chen et al., 2018). The products, such as highly oxygenated organic molecules (HOMs), from these aqueous-phase reactions would be conducive to elevating O:C (Molteni et al., 2018; Bianchi et al., 2019). On the other hand, the Fig. S7 showed that, the O:C ratio generally increased and the H:C ratio decreased during the day of 8:00–16:00 local time (LT), suggesting that SOA formation like photochemical process or mixing with more aged aerosols from regional sources was dominant during the day and outweighed the emissions POA (Sun et al., 2013).

To further investigate the pathways of OA factors, ions in the HR mass spectra were used to calculate the elemental ratios using the improved-ambient method (Canagaratna et al., 2015). The ratios were represented by the VK diagram in Fig. 8a (Heald et al., 2010) to show the OA evolution in the summertime of Handan. Based on our data, we found that HOA and COA factors (POA) are both located at the left-top corner with high H:C, low O:C and OSc below −1. Then, these POAs evolve toward the right bottom during the formation of SOA (Zhao et al., 2019). Functional groups are further added in Fig. 8a: only oxygen atoms to a carbon backbone results in a slope equal 0, while the replacement of a hydrogen atom with a carboxylic acid group (−COOH) results in a slope of −1 without fragmentation (Heald et al., 2010; Ng et al., 2011). As organic compounds are oxidized, a relatively flat slope of −0.19 for H:C versus O:C in this study suggests the importance of the addition of alcohol and/or peroxide (slope = 0) in OA aging with additional processes adding carboxylic acid and/or carboxyl groups. For SOA factors, fresh SOA factors are located in upper left region with high H:C and low O:C values compared with the other SOA factors. Although the primary-related SOA has the lower O:C than other SOAs, it still located closely to these two SOAs， which further indicates they might

have similar formation, compositions or transformation between these factors, which is consistent with the results from above section.

Table S3 present the comparison of average O:C (0.77 ±0.1) and H:C (1.58 ±0.1) for bulk OA in this study (three periods in Handan) with studies from China and other campaigns (four seasons in urban/suburban sites) based on the updated IA calibrations in Canagaratna et al. (2015). Briefly, OA in this study are at the higher end of O:C ranges reported in urban areas of China, and are comparable to the O:C ratios at the suburban sites, suggesting the OA was fairly oxidized in summer in the urban Handan.

1.5 f_{43} Versus f_{44}

Since the ion fragment with *m/z* = 44 and 43 are usually originated from different functional groups and the ratio changes as a function of atmospheric aging, researchers usually use the triangle plot of f_{44} versus f_{43} to characterize OA evolutions in the atmosphere. As shown in Fig. S12, POA and SOA factors fell into similar regions of f_{44} versus f_{43}, suggesting that OA factors identified by PMF were fairly similar in the summertime of Handan. The bottom region of the triangle was dominated by POA factors (including HOA and COA) with low f_{44} (about 0.05) and f_{43} of 0.06 to 0.08, indicating that they were freshly emitted and less oxidized. Comparatively, SOA factors are located in different regions: (1) the fresh SOA region with low f_{44} (<0.10), indicating they were relatively less oxidized compared to other SOA factors. (2) the region with high f_{44} (>0.17) than other OA factors, consistent with the fact that sqSOA and O_x-initiated SOA were surrogates of highly oxidized or regionally transported SOAs (Zhao et al., 2019); and (3) primary-related SOA region, showing freshly oxidized properties (f_{44} around 0.15). From the color plot of f_{29} (mainly f_{CHO+}), f_{CHO+} was observed highly correlated with formation of aged SOA factors.

References

Aiken, A. C., Salcedo, D., Cubison, M. J., Huffman, J. A., DeCarlo, P. F., Ulbrich, I. M., Docherty, K. S., Sueper, D., Kimmel, J. R., Worsnop, D. R., Trimborn, A., Northway, M., Stone, E. A., Schauer, J. J., Volkamer, R. M., Fortner, E., de Foy, B., Wang, J., Laskin, A., Shutthanandan, V., Zheng, J., Zhang, R., Gaffney, J., Marley, N. A., Paredes-Miranda, G., Arnott, W. P., Molina, L. T., Sosa, G., and Jimenez, J. L.: Mexico City aerosol analysis during MILAGRO using high resolution aerosol mass spectrometry at the urban supersite (T0) – Part 1: Fine particle composition and organic source apportionment, Atmos. Chem. Phys., 9, 6633–6653, https://doi.org/10.5194/acp-9-6633-2009, 2009.

Altieri K E, Carlton A G, Lim H J, et al. Evidence for oligomer formation in clouds: Reactions of isoprene oxidation products. Environmental science & technology, 40(16): 4956-4960, https://doi.org/10.1021/es052170n, 2006.

Ban-Weiss, G. A., J. P. McLaughlin, R. A. Harley, M. M. Lunden, T. W. Kirchstetter, A. J. Kean, A. W. Strawa, E. D. Stevenson, and G. R. Kendall, Long-term changes in emissions of nitrogen oxides and particulate matter from on-road gasoline and diesel vehicles, Atmos. Environ., 42(2), 220-232, https://doi.org/10.1016/j.atmosenv.2007.09.049, 2008.

Bianchi F, Kurtén T, Riva M, et al. Highly oxygenated organic molecules (HOM) from gas-phase autoxidation involving peroxy radicals: A key contributor to atmospheric aerosol. Chemical reviews, 119(6): 3472-3509. DOI: 10.1021/acs.chemrev.8b00395, 2019.

Budisulistiorini S H, Chen J, Itoh M, et al. Can Online Aerosol Mass Spectrometry Analysis Classify Secondary Organic Aerosol (SOA) and Oxidized Primary Organic Aerosol (OPOA)? A Case Study of Laboratory and Field Studies of Indonesian Biomass Burning. ACS Earth and Space Chemistry, 5(12): 3511-3522, https://doi.org/10.1021/acsearthspacechem.1c00319, 2021.

Canagaratna M R, Jayne J T, Ghertner D A, et al. Chase Studies of Particulate Emissions from in-use New York City Vehicles, Aerosol Science and Technology, 38:6, 555-573, DOI: 10.1080/02786820490465504，2004.

Canagaratna, M.R., Jimenez, J.L., Kroll, J.H., Chen, Q., Kessler, S.H., Massoli, P., Hildebrandt Ruiz, L., Fortner, E., Williams, L.R., Wilson, K.R., Surratt, J.D., Donahue, N.M., Jayne, J.T., Worsnop, D.R., 2015. Elemental ratio measurements of organic compounds using aerosol mass spectrometry: Characterization, improved calibration, and implications. Atmos. Chem. Phys. 15, 253–272. https://doi.org/10.5194/acp-15-253-2015

Chen T, Liu J , Liu Y , et al. Chemical characterization of submicron aerosol in summertime Beijing: A case study in southern suburbs in 2018. Chemosphere, 247:125918, 2020a

Chen, T., Liu, J., Ma, Q., Chu, B., Zhang, P., Ma, J., Liu, Y., Zhong, C., Liu, P., Wang, Y., Mu, Y., and He, H.: Measurement report: Effects of photochemical aging on the formation and evolution of summertime secondary aerosol in Beijing, Atmos. Chem. Phys. Discuss., https://doi.org/10.5194/acp-2020-792, in review, 2020b.

Chen, W., Ye, Y., Hu, W., Zhou, H., Pan, T., Wang, Y., Song, W., Song, Q., Ye, C., Wang, C., Wang, B., Huang, S., Yuan, B., Zhu, M., Lian, X., Zhang, G., Bi, X., Jiang, F., Liu, J., Canonaco, F., Prevot, A.S.H., Shao, M., Wang, X., 2021. Real-time characterization of aerosol compositions, sources and aging processes in Guangzhou during PRIDE-GBA 2018 campaign. J. Geophys. Res. Atmos. https://doi.org/10.1029/2021jd035114

Docherty, K. S., Aiken, A. C., Huffman, J. A., Ulbrich, I. M., DeCarlo, P. F., Sueper, D., Worsnop, D. R., Snyder, D. C., Peltier, R. E., Weber, R. J., Grover, B. D., Eatough, D. J., Williams, B. J., Goldstein, A. H., Ziemann, P. J., and Jimenez, J. L.: The 2005 Study of Organic Aerosols at Riverside (SOAR-1): instrumental intercomparisons and fine particle composition, Atmos. Chem. Phys., 11, 12387–12420, https://doi.org/10.5194/acp-11-12387-2011, 2011

Duan, J., Huang, R.-J., Li, Y., Chen, Q., Zheng, Y., Chen, Y., Lin, C., Ni, H., Wang, M., Ovadnevaite, J., Ceburnis, D., Chen, C., Worsnop, D.R., Hoffmann, T., O'Dowd, C., Cao, J.J., 2020. Summertime and wintertime atmospheric processes of secondary aerosol in Beijing Atmos. Chem. Phys. 20, 3793–3807.

Dzepina, K., Arey, J., Marr, L.C., Worsnop, D.R., Salcedo, D., Zhang, Q., Onasch, T.B., Molina, L.T., Molina, M.J., Jimenez, J.L., 2007. Detection of particle-phase polycyclic aromatic hydrocarbons in Mexico City using an aerosol mass spectrometer. Int. J. Mass Spectrom. 263, 152–170. https://doi.org/10.1016/j.ijms.2007.01.010

Elser, M., Huang, R.-J., Wolf, R., Slowik, J.G., Wang, Q., Canonaco, F., Li, G., Bozzetti, C., Daellenbach, K.R., Huang, Y., Zhang, R., Li, Z., Cao, J., Baltensperger, U., ElHaddad, I., Prevot, A.S.H., 2016. New insights into PM2.5 chemical composition and sources in two major cities in China during extreme haze events using aerosol mass spectrometry. Atmos. Chem. Phys. 16, 3207–3225.

Ge, X. L., Setyan, A., Sun, Y. L., and Zhang, Q.: Primary and secondary organic aerosols in Fresno, California during wintertime: Results from high resolution aerosol mass spectrometry, J. Geophys. Res., 117, D19301, https://doi.org/10.1029/2012JD018026, 2012.

Gu, Yifang; Huang, Ru-Jin; Li, Yongjie; Duan, Jing; Chen, Qi; Hu, Weiwei; Zheng, Yan; Lin, Chunshui; Ni, Haiyan; Dai, Wenting; Cao, Junji; Liu, Quan; Chen, Yang; Chen, Chunying; Ovadnevaite, Jurgita; Ceburnis, Darius; O'Dowd, Colin. Chemical nature and sources of fine particles in urban Beijing: Seasonality and formation mechanisms. Environment International, 2020, 140. DOI: 10.1016/j.envint.2020.105732

Gong, Z., Lan, Z., Xue, L., Zeng, L., He, L., and Huang, X.: Characterization of submicron aerosols in the urban outflow of the central Pearl River Delta region of China, Front. Env. Sci. Eng., 6, 725-733, https://doi.org/10.1007/s11783-012-0441-8, 2012

Hallquist, M., Wenger, J. C., Baltensperger, U., Rudich, Y., Simpson, D., Claeys, M., Dommen, J., Donahue, N. M., George, C., Goldstein, A. H., Hamilton, J. F., Herrmann, H., Hoffmann, T., Iinuma, Y., Jang, M., Jenkin, M. E., Jimenez, J. L., Kiendler-Scharr, A., Maenhaut, W., McFiggans, G., Mentel, Th. F., Monod, A., Prévôt, A. S. H., Seinfeld, J. H., Surratt, J. D., Szmigielski, R., and Wildt, J.: The formation, properties and impact of secondary organic aerosol: current and emerging issues, Atmos. Chem. Phys., 9, 5155–5236, https://doi.org/10.5194/acp-9-5155-2009, 2009.

Hayes, P. L., Ortega, A. M., Cubison, M. J., Froyd, K. D., Zhao, Y., Cliff, S. S., Hu, W. W., Toohey, D. W., Flynn, J. H., Lefer, B. L., Grossberg, N., Alvarez, S., Rappenglück, B., Taylor, J. W., Allan, J. D., Holloway, J. S., Gilman, J. B., Kuster, W. C., de Gouw, J. A., Massoli, P., Zhang, X., Liu, J., Weber, R. J., Corrigan, A. L., Russell, L. M., Isaacman, G., Worton, D. R., Kreisberg, N. M., Goldstein, A. H., Thalman, R., Waxman, E. M., Volkamer, R., Lin, Y. H., Surratt, J. D., Kleindienst, T. E., Offenberg, J. H., Dusanter, S., Griffith, S., Stevens, P. S., Brioude, J., Angevine, W. M., and Jimenez, J. L.: Organic

aerosol composition and sources in Pasadena, California, during the 2010 CalNex campaign, J. Geophys. Res.-Atmos., 118, 9233–9257, https://doi.org/10.1002/jgrd.50530, 2013.

He, L. Y., Huang, X. F., Xue, L., Hu, M., Lin, Y., Zheng, J., Zhang, R. Y., and Zhang, Y. H.: Submicron aerosol analysis and organic source apportionment in an urban atmosphere in Pearl River Delta of China using high-resolution aerosol mass spectrometry, J. Geophys. Res., 116, D12304, https://doi.org/10.1029/2010JD014566, 2011.

Heald, C.L., Kroll, J.H., Jimenez, J.L., Docherty, K.S., Decarlo, P.F., Aiken, A.C., Chen, Q., Martin, S.T., Farmer, D.K., Artaxo, P., 2010. A simplified description of the evolution of organic aerosol composition in the atmosphere. Geophys. Res. Lett. 37. https://doi.org/10.1029/2010GL042737

Herndon, S.C., Onasch, T.B., Wood, E.C., Kroll, J.H., Canagaratna, M.R., Jayne, J.T., Zavala, M.A., Knighton, W.B., Mazzoleni, C., Dubey, M.K., Ulbrich, I.M., Jimenez, J.L., Seila, R., de Gouw, J.A., de Foy, B., Fast, J., Molina, L.T., Kolb, C.E., Worsnop, D.R., 2008. Correlation of secondary organic aerosol with odd oxygen in Mexico City. Geophys. Res. Lett. 35. https://doi.org/10.1029/2008GL034058

Hu, J., Wang, P., Ying, Q., Zhang, H., Chen, J., Ge, X., Li, X., Jiang, J., Wang, S., Zhang, J., Zhao, Y., Zhang, Y., 2017. Modeling biogenic and anthropogenic secondary organic aerosol in China. Atmos. Chem. Phys. 17, 77–92.

Hu, W.W., Hu, M., Hu, W., Jimenez, J.L., Yuan, B., Chen, W., Wang, M., Wu, Y., Chen, C., Wang, Z., Peng, J., Zeng, L., Shao, M., 2016a. Chemical composition, sources, and aging process of submicron aerosols in Beijing: Contrast between summer and winter. J. Geophys. Res.-Atmos. 121, 1955–1977.

Hu, W., Hu, M., Hu, W.-W., Niu, H., Zheng, J., Wu, Y., Chen, W., Chen, C., Li, L., Shao, M., Xie, S., and Zhang, Y.: Characterization of submicron aerosols influenced by biomass burning at a site in the Sichuan Basin, southwestern China, Atmos. Chem. Phys., 16, 13213–13230, https://doi.org/10.5194/acp-16-13213-2016, 2016b

Huang, X.-F., He, L.-Y., Hu, M., Canagaratna, M. R., Sun, Y., Zhang, Q., Zhu, T., Xue, L., Zeng, L.-W., Liu, X.-G., Zhang, Y.-H., Jayne, J. T., Ng, N. L., and Worsnop, D. R.: Highly timeresolved chemical characterization of atmospheric submicron particles during 2008 Beijing Olympic Games using an Aerodyne High-Resolution Aerosol Mass Spectrometer, Atmos. Chem. Phys., 10, 8933–8945, https://doi.org/10.5194/acp-10-8933-2010, 2010.

Huang, X.-F., He, L.-Y., Hu, M., Canagaratna, M. R., Kroll, J. H., Ng, N. L., Zhang, Y. H., Lin, Y., Xue, L., Sun, T. L., Liu, X. G., Shao, M., Jayne, J. T., and Worsnop, D. R.: Characterization of submicron aerosols at a rural site in Pearl River Delta of China using an Aerodyne HighResolution Aerosol Mass Spectrometer, Atmos. Chem. Phys., 11, 1865-1877, https://doi.org/10.5194/acp-11-1865-2011, 2011.

Huang, X.-F., He, L.-Y., Xue, L., Sun, T.-L., Zeng, L.-W., Gong, Z.-H., Hu, M., and Zhu, T.: Highly time-resolved chemical characterization of atmospheric fine particles during 2010 Shanghai World Expo, Atmos. Chem. Phys., 12, 4897–4907, https://doi.org/10.5194/acp-12-4897-2012, 2012.

Huang, X.-F., Xue, L., Tian, X. D., Shao, W. W., Sun, T. L., Gong, Z. H., Ju, W. W., Jiang, B., Hu, M., and He, L. Y.: Highly time-resolved carbonaceous aerosol characterization in Yangtze River Delta of China: Composition, mixing state and secondary formation, Atmos. Environ., 64, 200–207, https://doi.org/10.1016/j.atmosenv.2012.09.059, 2013

Jimenez, J.L., Canagaratna, M.R., Donahue, N.M., Prevot, A.S.H., Zhang, Q., Kroll, J.H., DeCarlo, P.F., Allan, J.D., Coe, H., Ng, N.L., Aiken, A.C., Docherty, K.S., Ulbrich, I.M., Grieshop, A.P., Robinson, A.L., Duplissy, J., Smith, J.D., Wilson, K.R., Lanz, V.A., Hueglin, C., Sun, Y.L., Tian, J., Laaksonen, A., Raatikainen, T., Rautiainen, J., Vaattovaara, P., Ehn, M., Kulmala, M., Tomlinson, J.M., Collins, D.R., Cubison, M.J., Dunlea, J., Huffman, J.A., Onasch, T.B., Alfarra, M.R., Williams, P.I., Bower, K., Kondo, Y., Schneider, J., Drewnick, F., Borrmann, S., Weimer, S., Demerjian, K., Salcedo, D., Cottrell, L., Griffin, R., Takami, A., Miyoshi, T., Hatakeyama, S., Shimono, A., Sun, J.Y., Zhang, Y.M., Dzepina, K., Kimmel, J.R., Sueper, D., Jayne, J.T., Herndon, S.C., Trimborn, A.M., Williams, L.R., Wood, E.C., Middlebrook, A.M., Kolb, C.E., Baltensperger, U., Worsnop, D.R., 2009. Evolution of Organic Aerosols in the Atmosphere. Science. 326(5959), 1525–1529.

Kroll, J.H., Seinfeld, J.H., 2008. Chemistry of secondary organic aerosol: formation and evolution of low-volatility organics in the atmosphere. Atmos. Environ. 42, 3593-3624.

Kuang, Y., He, Y., Xu, W.Y., Yuan, B., Zhang, G., Ma, Z.Q., Wu, C.H., Wang, C.M., Wang, S.H., Zhang, S.Y., Tao, J.C., Ma, N., Su, H., Cheng, Y.F., Shao, M., Sun, Y.L., 2020. Photochemical aqueous-phase reactions induce rapid daytime formation of oxygenated organic aerosol on the North China Plain. Environ. Sci. Technol. 54(7), 3849–3860.

Lanz, V. A., Alfarra, M. R., Baltensperger, U., Buchmann, B., Hueglin, C., and Prévôt, A. S. H.: Source apportionment of sub- micron organic aerosols at an urban site by factor analytical mod- elling of aerosol mass spectra, Atmos. Chem. Phys., 7, 1503– 1522, doi:10.5194/acp-7-1503-2007, 2007.

Lee, B. P., Li, Y. J., Yu, J. Z., Louie, P. K. K., and Chan, C. K.: Characteristics of submicron particulate matter at the urban roadside in downtown Hong Kong – Overview of 4 months of continuous high-resolution aerosol mass spectrom- eter measurements, J. Geophys. Res.-Atmos., 120, 7040–7058, https://doi.org/10.1002/2015JD023311, 2015.

Li, H., Zhang, Q., Zhang, Q., Chen, C., Wang, L., Wei, Z., Zhou, S., Parworth, C., Zheng, B., Canonaco, F., Prévôt, A. S. H., Chen, P., Zhang, H., Wallington, T. J., and He, K.: Wintertime aerosol chemistry and haze evolution in an extremely polluted city of the North China Plain: significant contribution from coal and biomass combustion, Atmos. Chem. Phys., 17, 4751–4768, https://doi.org/10.5194/acp-17-4751-2017, 2017.

Li, Y. J., Lee, B. P., Su, L., Fung, J. C. H., and Chan, C. K.: Seasonal characteristics of fine particulate matter (PM) based on high-resolution time-of-flight aerosol mass spectrometric (HR-ToF-AMS) measurements at the HKUST Supersite in Hong Kong, Atmos. Chem. Phys., 15, 37-53, https://doi.org/10.5194/acp-15-37-2015, 2015.

Lim, Y. B., Tan, Y., and Turpin, B. J.: Chemical insights, explicit chemistry, and yields of secondary organic aerosol from OH radical oxidation of methylglyoxal and glyoxal in the aqueous phase, Atmos. Chem. Phys., 13, 8651–8667, https://doi.org/10.5194/acp-13-8651-2013, 2013.

Liu, Y., Siekmann, F., Renard, P., El Zein, A., Salque, G., El Haddad, I., Temime-Roussel, B., Voisin, D., Thissen, R., Monod, A., 2012. Oligomer and SOA formation through aqueous phase photooxidation of methacrolein and methyl vinyl ketone. Atmos. Environ. 49, 123-129.

Mohr, C., DeCarlo, P. F., Heringa, M. F., Chirico, R., Slowik, J. G., Richter, R., Reche, C., Alastuey, A., Querol, X., Seco, R., Peñuelas, J., Jiménez, J. L., Crippa, M., Zimmermann, R., Baltensperger, U., and Prévôt, A. S. H.: Identification and quantification of organic aerosol from cooking and other sources in Barcelona using aerosol mass spectrometer data, Atmos. Chem. Phys., 12, 1649–1665, https://doi.org/10.5194/acp-12-1649-2012, 2012.

Molteni, U., Bianchi, F., Klein, F., El Haddad, I., Frege, C., Rossi, M.J., Dommen, J., Baltensperger, U., 2018. Formation of highly oxygenated organic molecules from aromatic compounds. Atmos. Chem. Phys. 18, 1909-1921.

Ng, N. L., Canagaratna, M. R., Zhang, Q., Jimenez, J. L., Tian, J., Ulbrich, I. M., Kroll, J. H., Docherty, K. S., Chhabra, P. S., Bahreini, R., Murphy, S. M., Seinfeld, J. H., Hildebrandt, L., Donahue, N. M., DeCarlo, P. F., Lanz, V. A., Prévôt, A. S. H., Dinar, E., Rudich, Y., and Worsnop, D. R.: Organic aerosol components observed in Northern Hemispheric datasets from Aerosol Mass Spectrometry, Atmos. Chem. Phys., 10, 4625–4641, https://doi.org/10.5194/acp-10-4625-2010, 2010.

Ng, N. L., Canagaratna, M. R., Jimenez, J. L., Chhabra, P. S., Se- infeld, J. H., and Worsnop, D. R.: Changes in organic aerosol composition with aging inferred from aerosol mass spectra, At- mos. Chem. Phys., 11, 6465–6474, https://doi.org/10.5194/acp- 11-6465-2011, 2011.

Qin, Y. M., Tan, H. B., Li, Y. J., Schurman, M. I., Li, F., Canonaco, F., Prévôt, A. S. H., and Chan, C. K.: Impacts of traffic emissions on atmospheric particulate nitrate and organics at a downwind site on the periphery of Guangzhou, China, Atmos. Chem. Phys., 17, 10245–10258, https://doi.org/10.5194/acp-17-10245-2017, 2017.

Rivellini, L.-H., Adam, M. G., Kasthuriarachchi, N., and Lee, A. K. Y.: Characterization of carbonaceous aerosols in Singapore: insight from black carbon fragments and trace metal

ions detected by a soot particle aerosol mass spectrometer, Atmos. Chem. Phys., 20, 5977–5993, https://doi.org/10.5194/acp-20-5977-2020, 2020.

Schöne, L. and Herrmann, H.: Kinetic measurements of the reactivity of hydrogen peroxide and ozone towards small atmospherically relevant aldehydes, ketones and organic acids in aqueous solutions, Atmos. Chem. Phys., 14, 4503–4514, https://doi.org/10.5194/acp-14-4503-2014, 2014.

Sun, Y. L., Zhang, Q., Anastasio, C., and Sun, J.: Insights into secondary organic aerosol formed via aqueous-phase reactions of phenolic compounds based on high resolution mass spectrometry, Atmos. Chem. Phys., 10, 4809–4822, https://doi.org/10.5194/acp-10-4809-2010, 2010.

Sun, Y. L., Wang, Z. F., Fu, P. Q., Yang, T., Jiang, Q., Dong, H. B., Li, J., and Jia, J. J.: Aerosol composition, sources and processes during wintertime in Beijing, China, Atmos. Chem. Phys., 13, 4577–4592, https://doi.org/10.5194/acp-13-4577-2013, 2013.

Sun, Y. L., Wang, Z. F., Du, W., Zhang, Q., Wang, Q. Q., Fu, P. Q., Pan, X. L., Li, J., Jayne, J., and Worsnop, D. R.: Long-term real-time measurements of aerosol particle composition in Beijing, China: seasonal variations, meteorological effects, and source analysis, Atmos. Chem. Phys., 15, 10149–10165, https://doi.org/10.5194/acp-15-10149-2015, 2015.

Sun, Y., Du, W., Fu, P., Wang, Q., Li, J., Ge, X., Zhang, Q., Zhu, C., Ren, L., Xu, W., Zhao, J., Han, T., Worsnop, D. R., and Wang, Z.: Primary and secondary aerosols in Beijing in winter: sources, variations and processes, Atmos. Chem. Phys., 16, 8309–8329, https://doi.org/10.5194/acp-16-8309-2016, 2016.

Sun, Y., Xu, W., Zhang, Q., Jiang, Q., Canonaco, F., Prévôt, A.S.H., Fu, P., Li, J., Jayne, J., Worsnop, D.R., Wang, Z., 2018. Source apportionment of organic aerosol from 2-year highly time-resolved measurements by an aerosol chemical speciation monitor in Beijing, China. Atmos. Chem. Phys. 18, 8469–8489. https://doi.org/10.5194/acp-18-8469-2018

Wang, L. T., Wei, Z., Yang, J., Zhang, Y., Zhang, F. F., Su, J., Meng, C. C., and Zhang, Q.: The 2013 severe haze over southern Hebei, China: model evaluation, source apportionment, and policy implications, Atmos. Chem. Phys., 14, 3151–3173, doi:10.5194/acp-14-3151-2014, 2014.

Wang J, Ye J, Zhang Q, et al. Aqueous production of secondary organic aerosol from fossil-fuel emissions in winter Beijing haze. Proceedings of the National Academy of Sciences, 118(8): e2022179118, https://doi.org/10.1073/pnas.2022179118, 2021.

Waxman, E.M., Dzepina, K., Ervens, B., Lee-Taylor, J., Aumont, B., Jimenez, J.L., Madronich, S., Volkamer, R., 2013. Secondary organic aerosol formation from semi- and intermediate-volatility organic compounds and glyoxal: relevance of O/C as a tracer for aqueous multiphase chemistry. Geophys. Res. Lett. 40, 978-982.

635 Xu, S., Liu, W., Tao, and S. Emission of Polycyclic Aromatic Hydrocarbons in China. Biophys.
636 Process. Anthropog. Org. Compd. Environ. Syst. 40, 267–281.
637 https://doi.org/10.1002/9780470944479.ch11, 2006.

638 Xu, J., Shi, J., Zhang, Q., Ge, X., Canonaco, F., Prévôt, A. S. H., Vonwiller, M., Szidat, S., Ge,
639 J., Ma, J., An, Y., Kang, S., and Qin, D.: Wintertime organic and inorganic aerosols in
640 Lanzhou, China: sources, processes, and comparison with the results during summer,
641 Atmos. Chem. Phys., 16, 14937–14957, https://doi.org/10.5194/acp-16-14937-2016,
642 2016.

643 Xu W, Han T, Du W, et al. Effects of aqueous-phase and photochemical processing on
644 secondary organic aerosol formation and evolution in Beijing, China. Environmental
645 Science & Technology, 51(2): 762-770, https://doi.org/10.1021/acs.est.6b04498, 2017.

646 Xu, W., Sun, Y., Wang, Q., Zhao, J., Wang, J., Ge, X., Xie, C., Zhou, W., Du, W., Li, J., Fu,
647 P., Wang, Z., Worsnop, D. R., Coe, H., Changes in aerosol chemistry from 2014 to 2016
648 in winter in Beijing: Insights from high-resolution aerosol mass spectrometry. J. Geophys.
649 Res.-Atmos. 124, 1132-1147, 2019a.

650 Xu, W., Xie, C., Karnezi, E., Zhang, Q., Wang, J., Pandis, S. N., Ge, X., Zhang, J., An, J.,
651 Wang, Q., Zhao, J., Du, W., Qiu, Y., Zhou, W., He, Y., Li, Y., Li, J., Fu, P., Wang, Z.,
652 Worsnop, D. R., and Sun, Y.: Summertime aerosol volatility measurements in Beijing,
653 China, Atmos. Chem. Phys., 19, 10205–10216, https://doi.org/10.5194/acp-19-10205-
654 2019, 2019b.

655 Zhang, Q., Jimenez, J. L., Canagaratna, M. R., et al.: Ubiquity and dominance of oxygenated
656 species in organic aerosols in anthropogenically-influenced Northern Hemisphere
657 midlatitudes, Geophys. Res. Lett., 34, L13801, doi:10.1029/2007GL029979, 2007.

658 Zhang, J. K., Sun, Y., Liu, Z. R., Ji, D. S., Hu, B., Liu, Q., and Wang, Y. S.: Characterization
659 of submicron aerosols during a month of serious pollution in Beijing, 2013, Atmos. Chem.
660 Phys., 14, 2887–2903, https://doi.org/10.5194/acp-14-2887-2014, 2014.

661 Zhang, X., Xu, J., Kang, S., Zhang, Q., and Sun, J.: Chemical characterization and sources of
662 submicron aerosols in the northeastern Qinghai–Tibet Plateau: insights from high-
663 resolution mass spectrometry, Atmos. Chem. Phys., 19, 7897–7911,
664 https://doi.org/10.5194/acp-19-7897- 2019, 2019.

665 Zhang, Z., Zhu, W., Hu, M., Liu, K., Wang, H., Tang, R., Shen, R., Yu, Y., Tan, R., Song, K.,
666 Li, Y., Zhang, W., Zhang, Z., Xu, H., Shuai, S., Li, S., Chen, Y., Li, J., Wang, Y., and
667 Guo, S.: Formation and evolution of secondary organic aerosols derived from urban-
668 lifestyle sources: vehicle exhaust and cooking emissions, Atmos. Chem. Phys., 21,
669 15221–15237, https://doi.org/10.5194/acp-21-15221-2021, 2021.

670 Zhao L , Wang L , Tan J , et al. Changes of chemical composition and source apportionment of
671 PM2.5 during 2013-2017 in urban Handan, China. Atmospheric Environment,
672 206(JUN.):119-131, 2019

673 Zhou, S., Collier, S., Jaffe, D. A., Briggs, N. L., Hee, J., Sedlacek III, A. J., Kleinman, L.,
674 Onasch, T. B., and Zhang, Q.: Regional influence of wildfires on aerosol chemistry in the
675 western US and insights into atmospheric aging of biomass burning organic aerosol,
676 Atmos. Chem. Phys., 17, 2477–2493, https://doi.org/10.5194/acp-17-2477-2017, 2017.